Supplement of Atmos. Chem. Phys., 16, 5399–5411, 2016
http://www.atmos-chem-phys.net/16/5399/2016/
doi:10.5194/acp-16-5399-2016-supplement
© Author(s) 2016. CC Attribution 3.0 License.

Supplement of

Size distribution and mixing state of black carbon particles during a heavy air pollution episode in Shanghai

Xianda Gong et al.

Correspondence to: Xin Yang (yangxin@fudan.edu.cn)

The copyright of individual parts of the supplement might differ from the CC-BY 3.0 licence.

1. SP2 data analysis and a way to enhance the LEO-fit accuracy

The SP2 data were analyzed using PSI v4.100 (Martin Gysel, Paul Scherrer Institute, 5232 Villigen, Switzerland) for the IGOR Pro software package (Wavemetrics, Inc., Portland, OR, USA).

The small particles are not necessarily heated to full incandescence in SP2. Therefore, one can get a peak that is smaller than it should be for a small mass of BC because the particle is not getting sufficiently hot. Furthermore, a high-gain on the narrowband detector, as used in this work, can introduce a decrease for the smallest particle sizes. The color ratio could possibly help with this issue. The color ratio was calculated from the ratio of the broadband to narrowband signals (Moteki and Kondo, 2010). We excluded BC-containing particles with color ratio in excess of 3.0 from analysis. This improved the LEO-fit accuracy, especially for small core rBC-containing particles.

2. Biomass burning black carbon (BBBC) particles classification criteria

To better classify BBBC particles, we combined ART-2a and ion-marker methods to validate the classification. We have done a lab study and a field measurement on the chemistry of biomass burning (mostly crop straw burning in China) BC-containing particles (Huo et al., 2015). Briefly, in addition to the black carbon fragment ions (Cn^+ and Cn^-) in both positive and negative ion mass spectra, +39 (K^+), -26 (CN^-), -42 (CNO^-) were used as the most important tracers for BBBC particles. Given the extremely high detection sensitivity of potassium (due to the high ionization cross-section of potassium at 266 nm) in SPAMS, it showed up in most mass spectra. The criterion for attributing the potassium signal to BBBC particles was that +39 (K^+) signal had to have the peak area of more than 1000, while the peak area of +56 (CaO^+/Fe^+) and -76 (SiO_3^-) had to be less than 50. Indeed, the paucity of Si, Ca and Fe is the major characteristic of biomass burning particles compared to coal burning particles (Pekney et al., 2006;Bein et al., 2007). Because of the K-rich nature of biomass burning material, +113 (K_2Cl^+) or +213 ($K_3SO_4^+$) were constantly observed in the mass spectra of biomass burning particles by ATOFMS. These ions could be used as markers for BBBC particles instead of +39 (K^+) to confirm our assignments of particles to the BBBC class. Lastly, -71 ($C_3H_3O_2^-$), as a significant fragment of levoglucosan, was an additional marker used to confirm our classification. We have applied the above criteria when regrouping the ART-2a results.

Table S1. Symbols and abbreviations

Symbol or abbreviation	Meaning
BC	Black carbon
rBC	Refractory black carbon
D_c	The black carbon core diameter
D_p	The entire particle diameter
D_{ME}	Mass equivalent diameter
D_{va}	The vacuum aerodynamic diameter
SP2	Single-particle soot photometer
SPAMS	Single particle aerosol mass spectrometer
sccm	Standard cubic centimeter per minute
ACT	Absolute coating thickness
RCT	Relative coating thickness

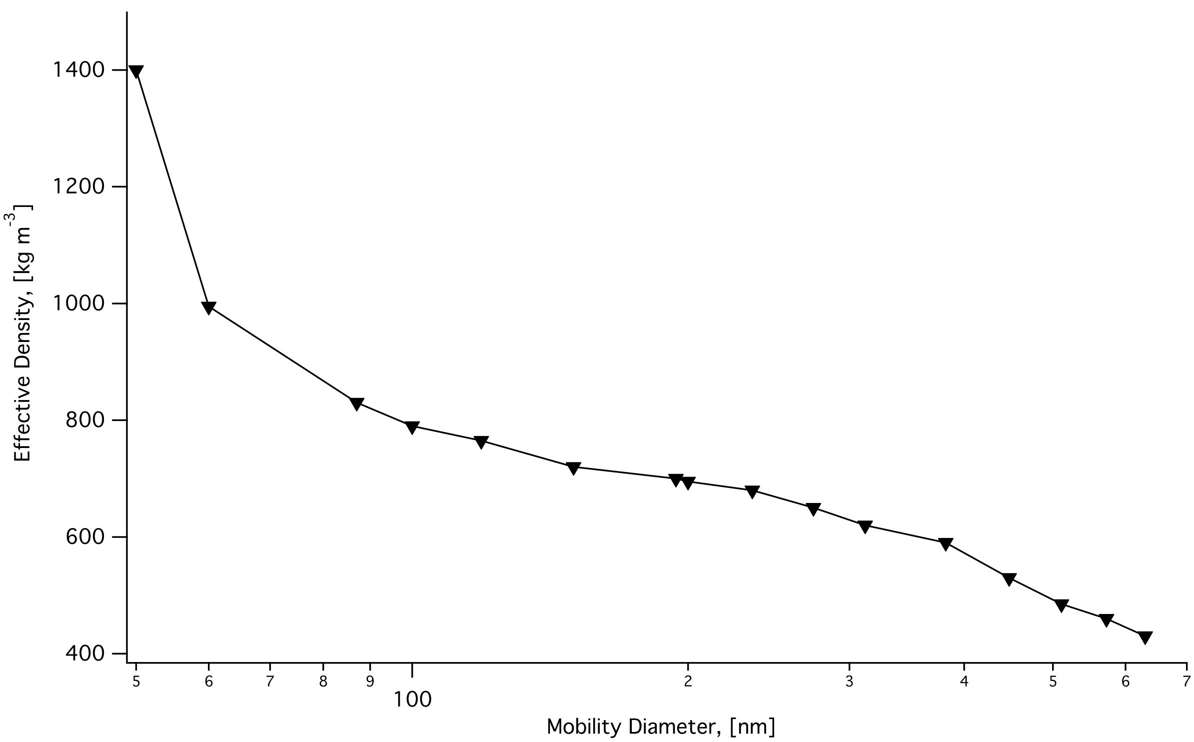

Figure S1. Effective density of Aquadag® black carbon as a function of mobility diameter.

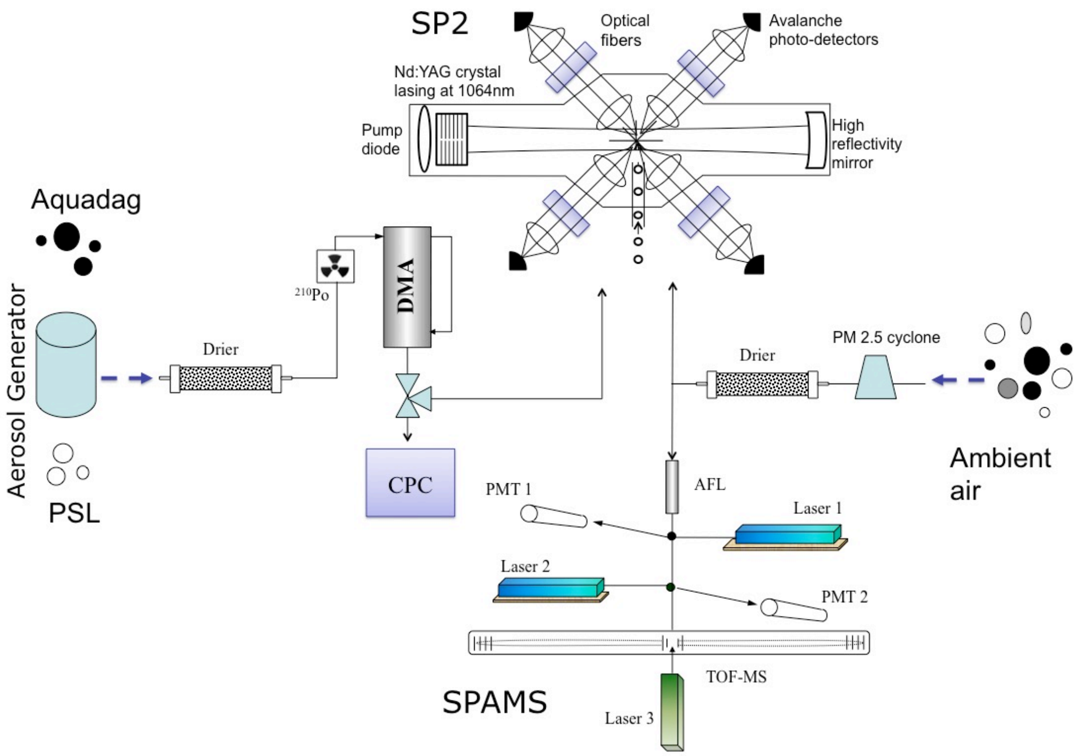

Figure S2. A schematic diagram of the calibration and measurement system. The DMA, CPC, SP2 and SPAMS represent Differential Mobility Analyzer, Condensation Particle Counter, Single Particle Soot Photometer, and Single Particle Aerosol Mass Spectrometer, respectively.

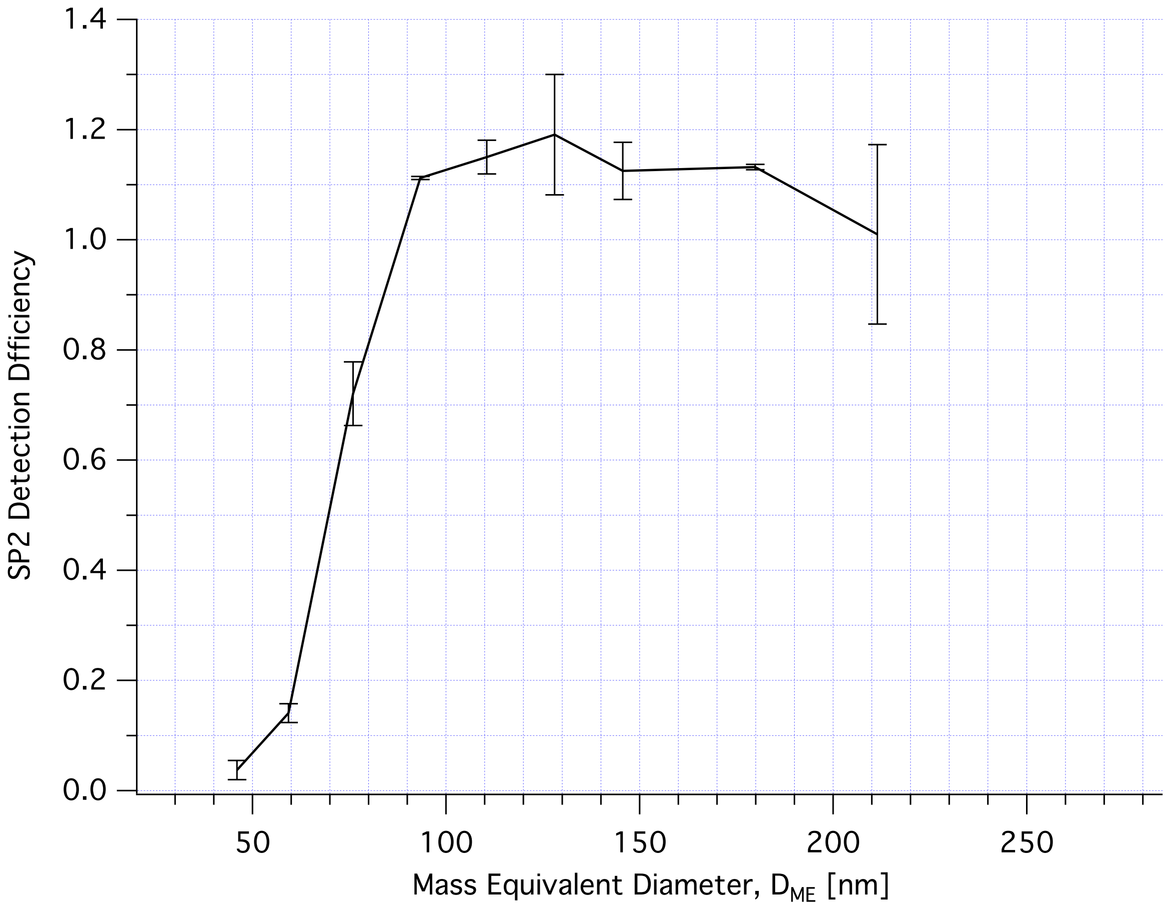

Figure S3. The average detection efficiencies in each rBC size-bin at a fixed laser intensity (1750 mA). Whiskers represent the standard deviation of the values in each size bin. In order to understand the mass and number size distribution of ambient rBC particles, here we transformed the mass equivalent diameter (D_{ME}) of Aquadag® BC to D_{ME} of ambient rBC according to their mass and different density. The detection efficiency of D_{ME} = 45 nm rBC was about 3.7%. The detection efficiency of 50% corresponded to D_{ME} = 75 nm.

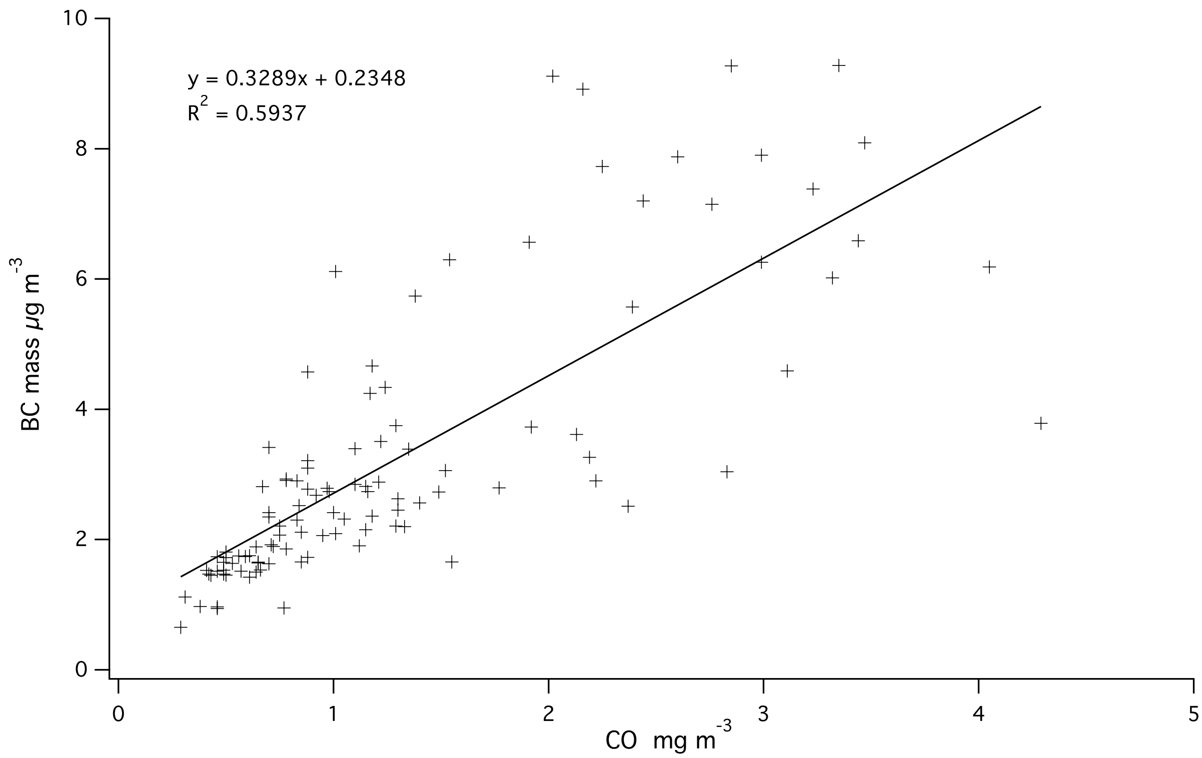

Figure S4. A comparison between the measured CO and rBC mass concentrations.

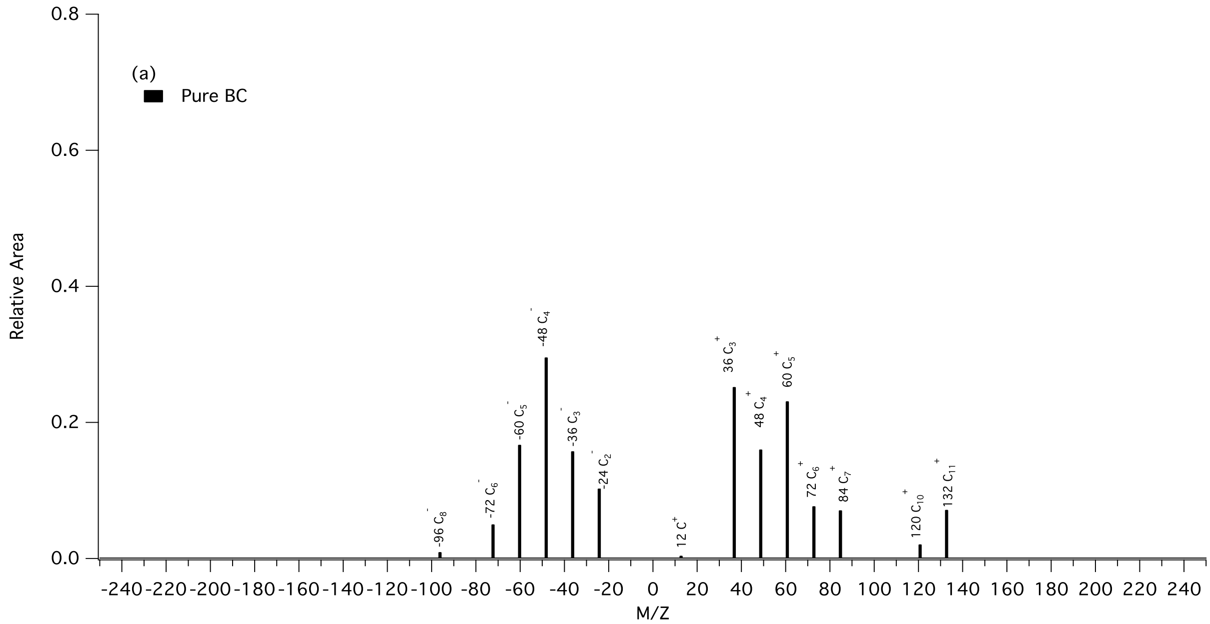
(a)
Pure BC
Relative Area
M/Z
-96 C8
-72 C6
-60 C5
-48 C4
-36 C3
-24 C2
12 C+
36 C3+
48 C4+
60 C5+
72 C6+
84 C7+
120 C10+
132 C11+

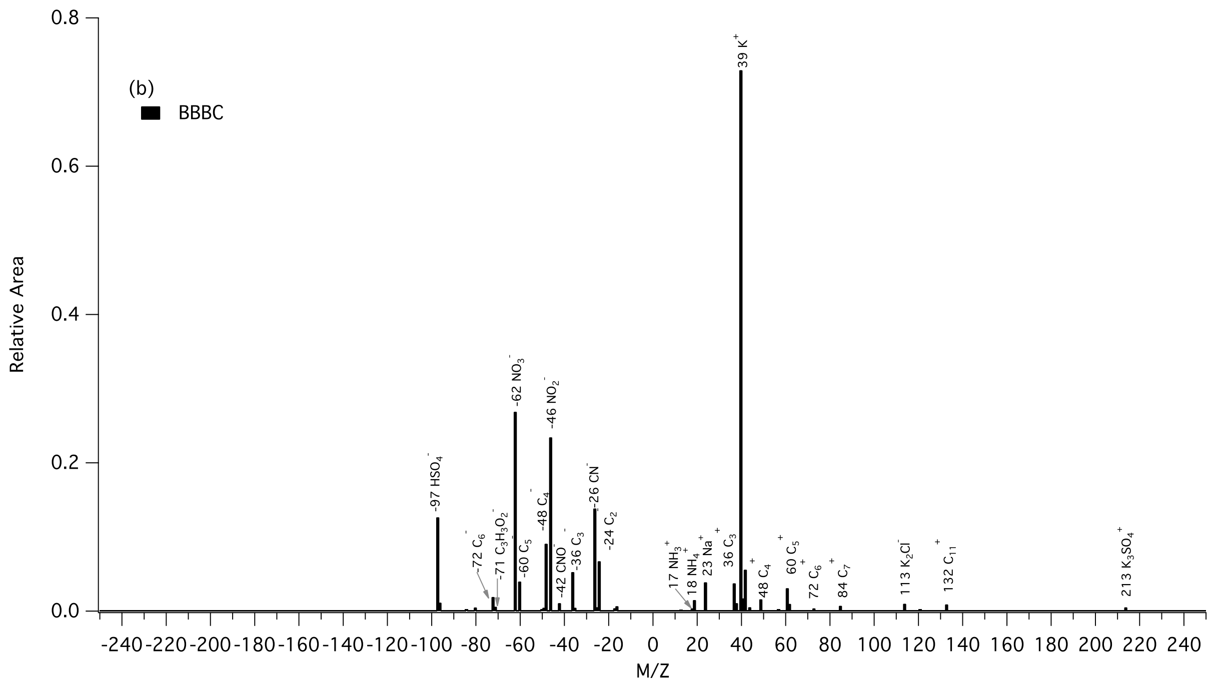
(b)
BBBC
Relative Area
M/Z
-97 HSO4-
-72 C6-
-71 C3H3O2-
-62 NO3-
-60 C5
-48 C4-
-46 NO2-
-42 CNO-
-36 C3-
-26 CN-
-24 C2
17 NH3+
18 NH4+
23 Na+
36 C3+
39 K+
48 C4+
60 C5+
72 C6+
84 C7+
113 K2Cl+
132 C11+
213 K3SO4+

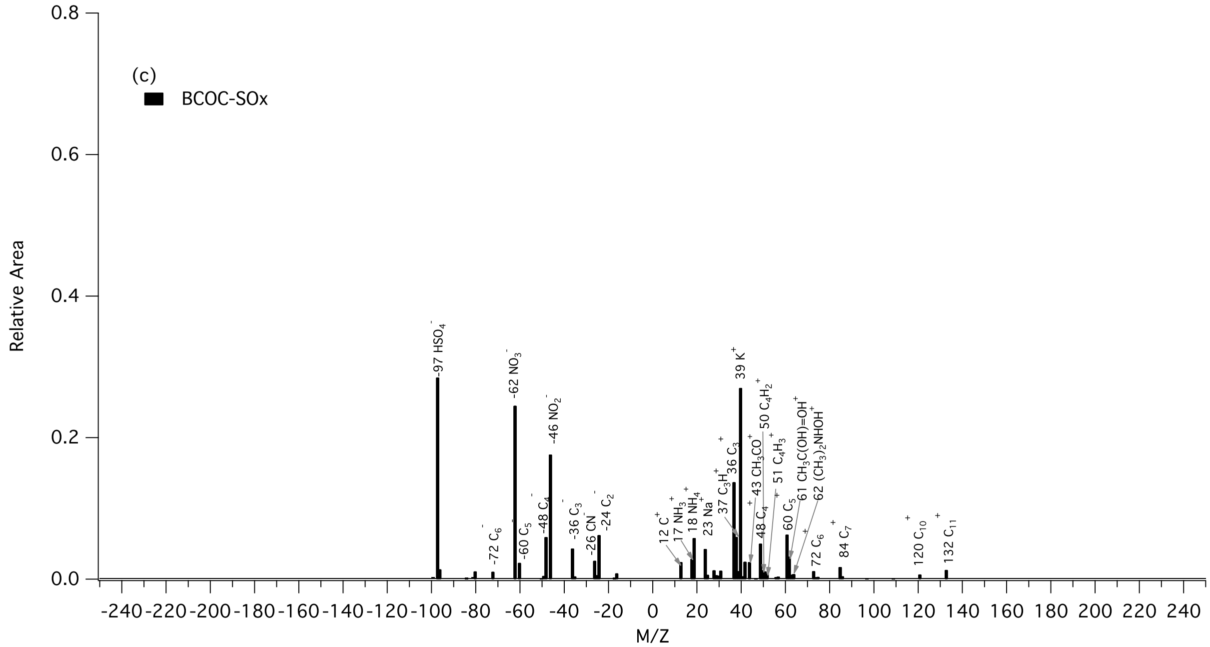
(c)
BCOC-SOx
Relative Area
M/Z
-97 HSO4-
-72 C6-
-62 NO3-
-60 C5-
-48 C4-
-46 NO2-
-36 C3-
-26 CN-
-24 C2-
12 C+
17 NH3+
18 NH4+
23 Na+
37 C3H+
36 C3+
39 K+
43 CH3CO+
48 C4+
50 C4H2+
51 C4H3+
60 C5+
61 CH3C(OH)=OH+
62 (CH3)2NHOH+
72 C6+
84 C7+
120 C10+
132 C11+

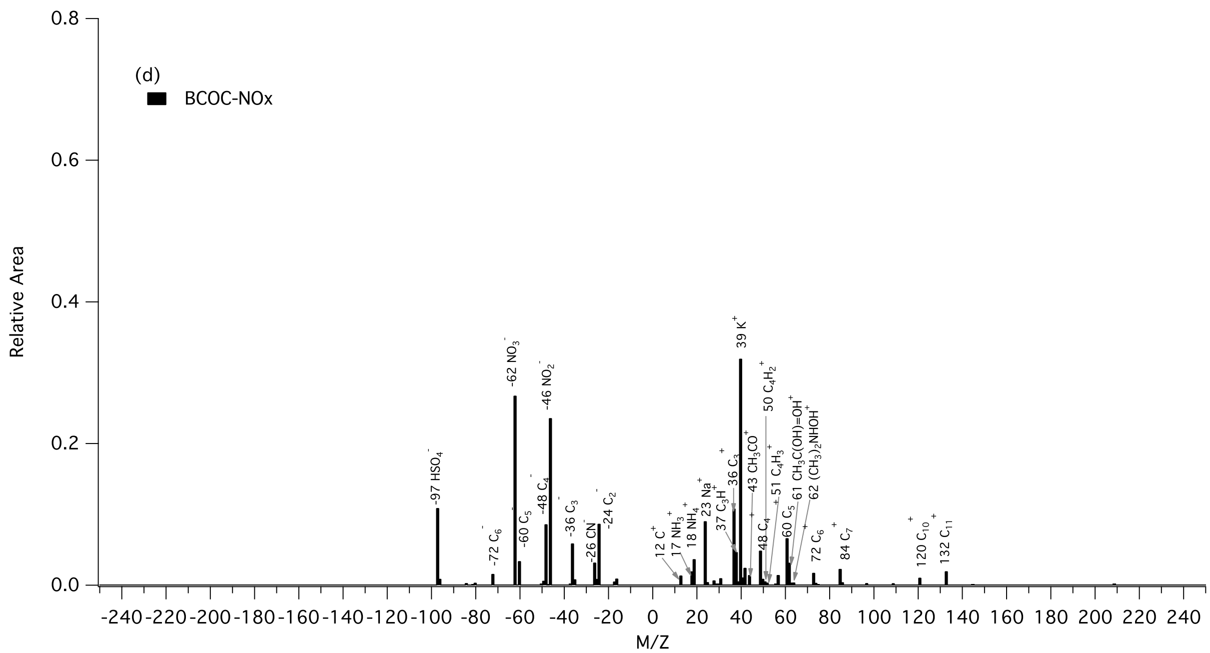
(d)
BCOC-NOx
Relative Area
M/Z
-97 HSO4-
-72 C6-
-62 NO3-
-60 C5-
-48 C4-
-46 NO2-
-36 C3-
-26 CN-
-24 C2-
12 C+
17 NH3+
18 NH4+
23 Na+
37 C3H+
36 C3+
39 K+
43 CH3CO+
48 C4+
50 C4H2+
51 C4H3+
60 C5+
61 CH3C(OH)=OH+
62 (CH3)2NHOH+
72 C6+
84 C7+
120 C10+
132 C11+

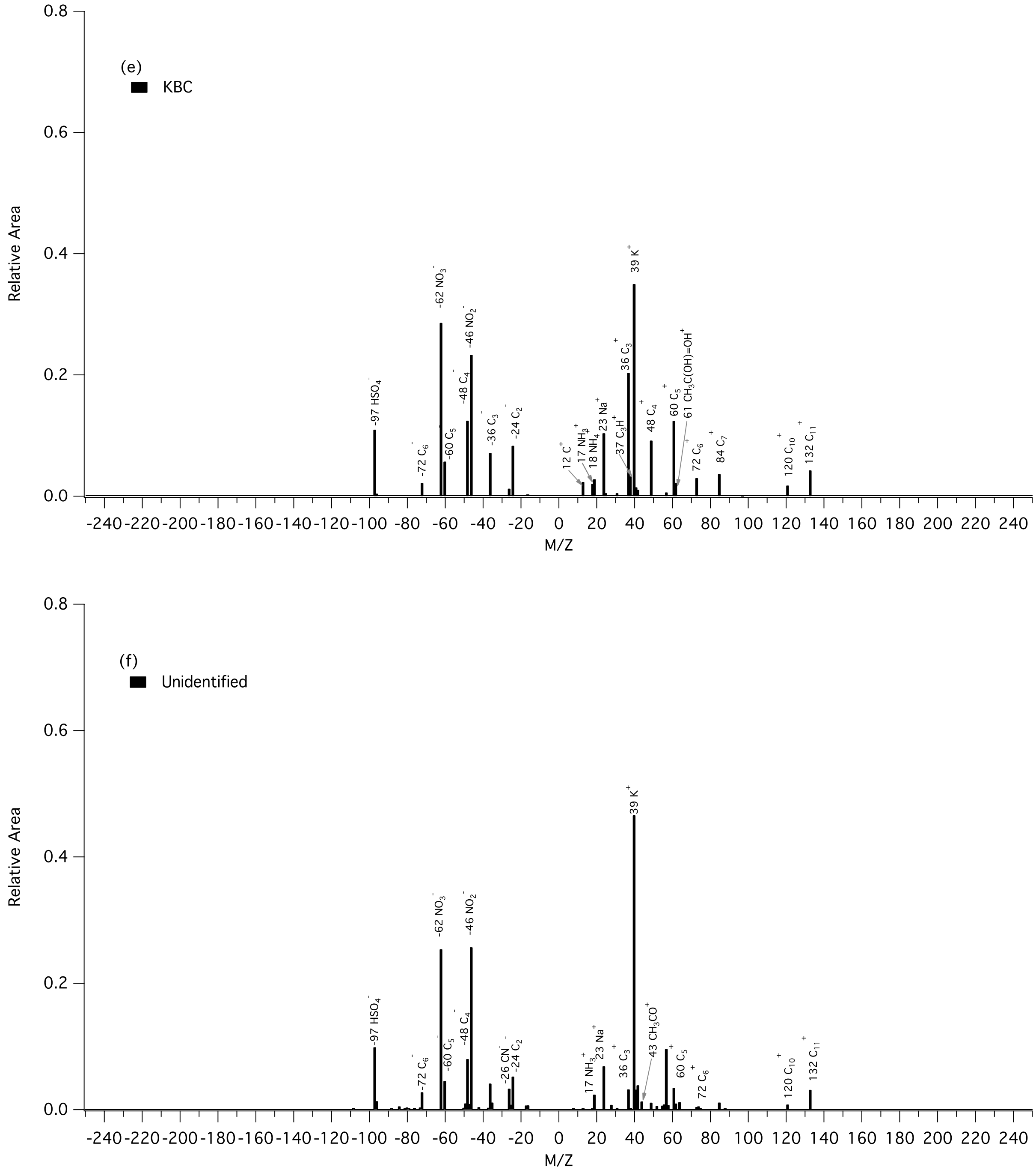

Figure S5. Averaged mass spectra of different types of BC-containing particles. Major peaks are labeled with the most probable assignments.

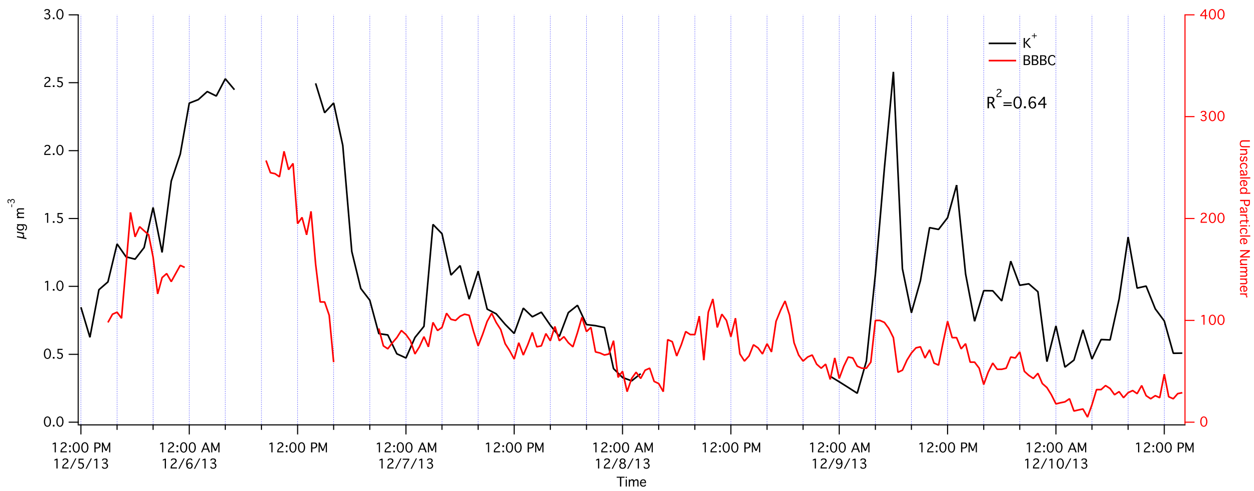

Figure S6. Temporal variations of K^+ mass concentration in particles (measured with MARGA) and biomass burning BC-containing particles (measured with SPAMS).

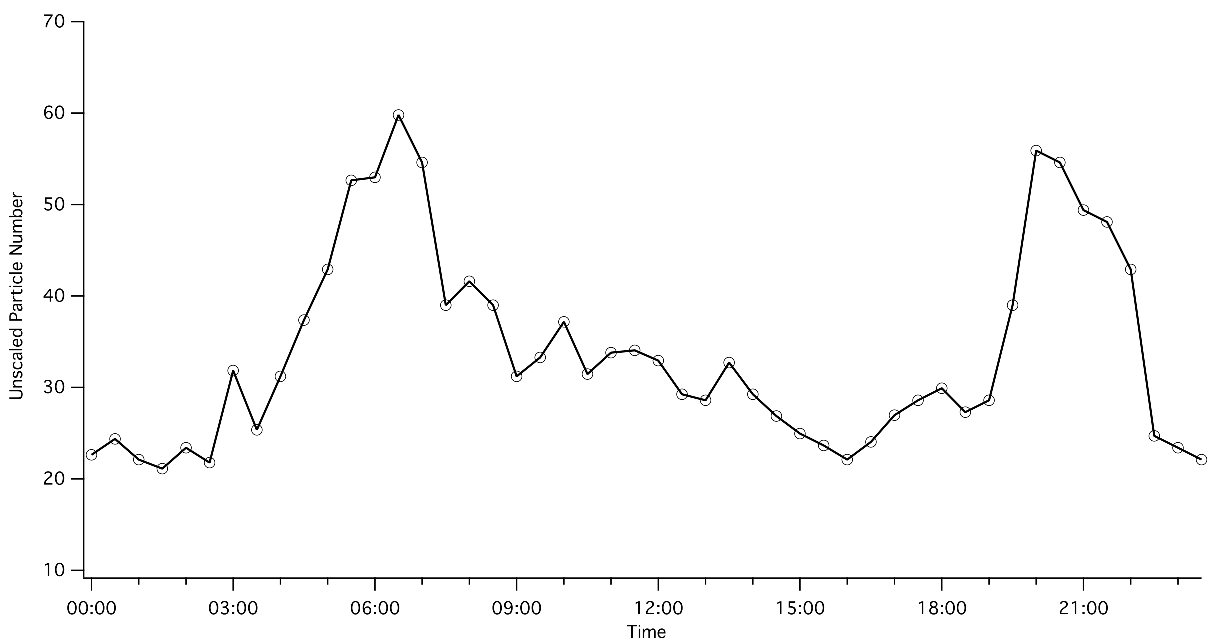

Figure S7. Diurnal variation of KBC particles measured with SPAMS.

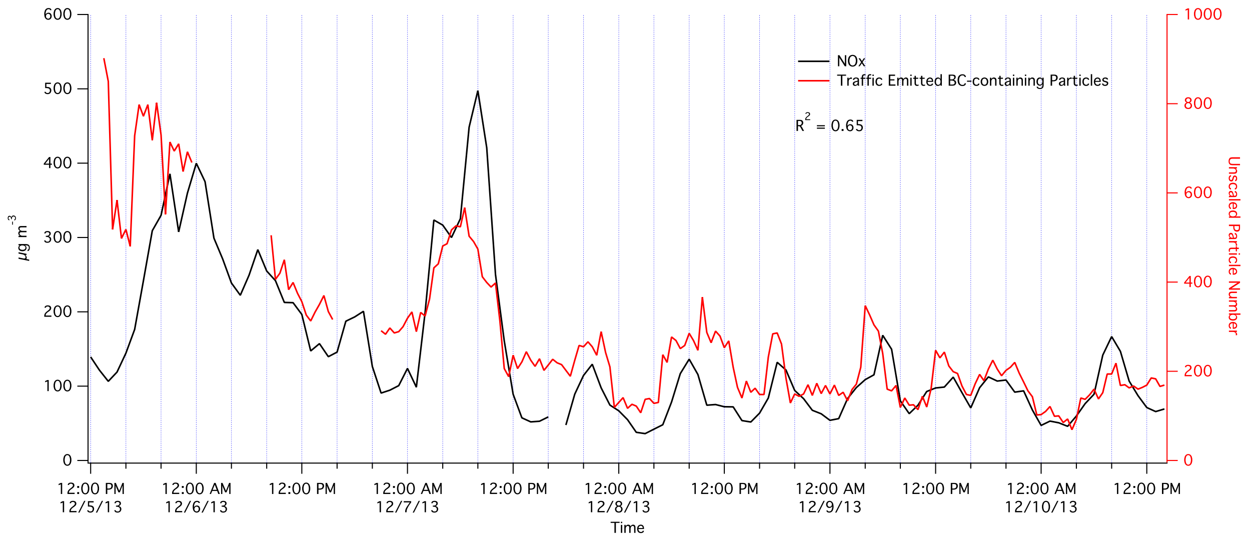

Figure S8. Temporal variation of NOx mass concentration and traffic-emitted BC-containing particles measured with SPAMS.

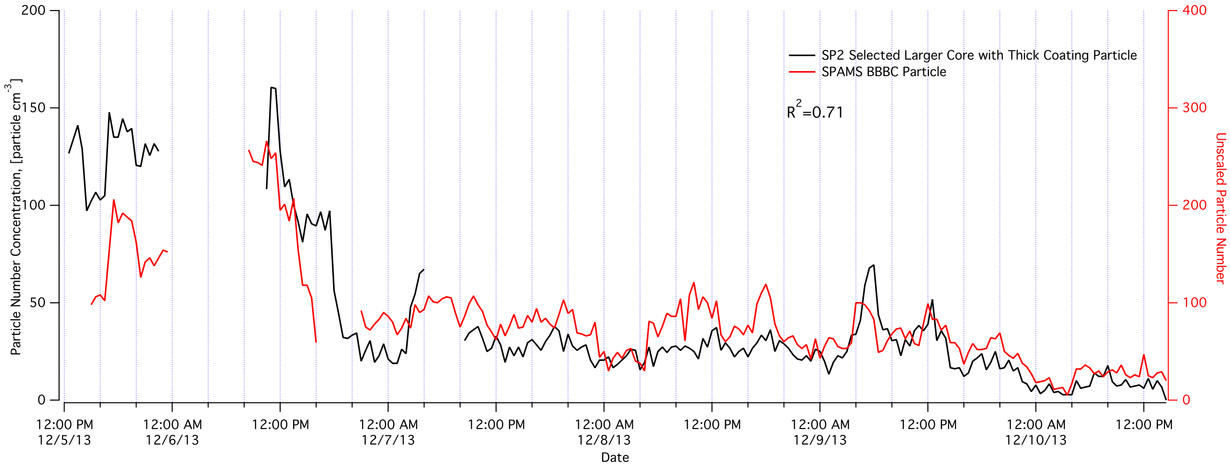

Figure S9. A comparison of the SPMAS-detected and SP2-detected biomass burning BC-containing particles.

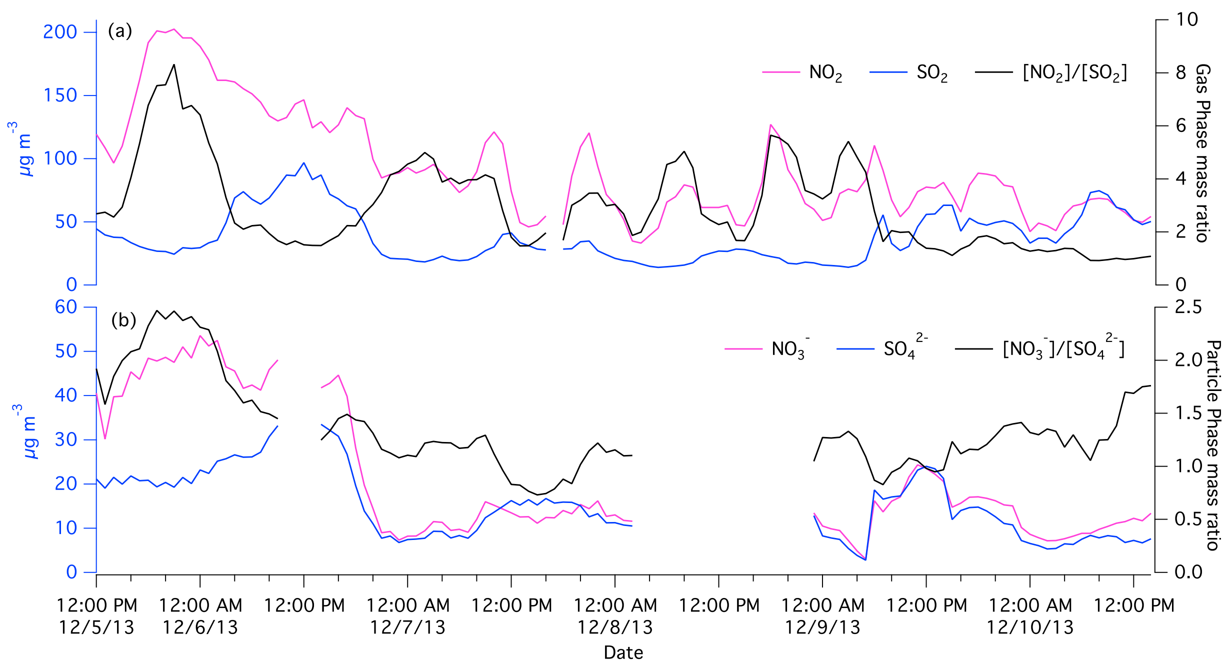

Figure S10. (a) Temporal variations of the NO_2 and SO_2 mass concentration in the atmosphere and mass ration of NO_2/SO_2 with 60 min resolution. (b) Temporal variation of NO_3^- and SO_4^{2-} mass concentration in particles and mass ratio of NO_3^-/SO_4^{2-} with 60 min resolution.

References

Bein, K. J., Zhao, Y., Johnston, M. V., and Wexler, A. S.: Identification of sources of atmospheric PM at the Pittsburgh Supersite—Part III: Source characterization, Atmos. Environ., 41, 3974-3992, doi:10.1016/j.atmosenv.2007.01.039, 2007.

Huo, J., Lu, X., Wang, X., Chen, H., Ye, X., Gao, S., Gross, D. S., Chen, J., and Yang, X.: Online single particle analysis of chemical composition and mixing state of crop straw burning particles: from laboratory study to field measurement, Frontiers of Environmental Science & Engineering, 10, 244-252, doi:10.1007/s11783-015-0768-z, 2015.

Moteki, N., and Kondo, Y.: Dependence of laser-induced incandescence on physical properties of black carbon aerosols: Measurements and theoretical interpretation, Aerosol Sci. Technol., 44, 663-675, doi: 10.1080/02786826.2010.484450, 2010.

Pekney, N. J., Davidson, C. I., Bein, K. J., Wexler, A. S., and Johnston, M. V.: Identification of sources of atmospheric PM at the Pittsburgh Supersite, Part I: Single particle analysis and filter-based positive matrix factorization, Atmos. Environ., 40, Supplement 2, 411-423, doi:10.1016/j.atmosenv.2005.12.072, 2006.